Large-Scale Fabrication of Wafer-Size Colloidal Crystals, Macroporous Polymers and Nanocomposites by Spin-Coating

Peng Jiang* and Michael J. McFarland

Contribution from the Corning Science and Technology, Corning Incorporated, Corning, New York 14831

Received May 18, 2004; E-mail: pjiang@princeton.edu

Abstract: This paper reports a simple spin-coating technique for rapidly fabricating three types of technologically important materials—colloidal crystal, macroporous polymer, and polymeric nanocomposite, each with high crystalline qualities and wafer-scale sizes. Dispersion of monodisperse silica colloids in triacrylate monomers is spin-coated onto a variety of substrates. Shear-induced ordering and subsequent polymerization lead to the formation of three-dimensionally (3D) ordered colloidal crystals trapped inside a polymer matrix. The thickness of as-synthesized colloidal crystal-polymer nanocomposite is highly uniform and can be controlled simply by changing the spin speed and time. Selective removal of the polymer matrix and silica spheres lead to the formation of large-area colloidal crystals and macroporous polymers, respectively. The wafer-scale process is compatible with standard semiconductor microfabrication, as multiple micrometer-sized patterns can be created simultaneously for potential device applications. Normal-incidence transmission spectra in the visible and near-infrared regions show distinct peaks due to Bragg diffraction from 3D ordered structures. The spin-coating process opens a new route to the fundamental studies of shear-induced crystallization, melting and relaxation.

Introduction

Colloidal crystals, three-dimensional (3D) periodic structures formed from monodisperse colloids,[1,2] have been extensively explored due to their important applications as diffractive optical devices,[3,4] chemical and bio-sensor,[5–8] and high-density magnetic and optical data recording materials.[9–11] They also serve as model systems for fundamental studies of crystallization and melting.[12–14] Recently, they have attracted renewed interest, mainly because they provide a much simpler, faster, and cheaper approach than complex semiconductor nanolithography techniques to create 3D photonic crystals working in the optical wavelength range.[15–17]

A variety of methods, such as gravity sedimentation,[18] electrostatic repulsion,[1,19,20] template assisted assembly,[21,22] physical confinement,[2,23] capillary forces induced convective self-assembly,[15,24,25] and electric field induced assembly,[26,27] have been developed to create colloidal crystals with millimeter to centimeter-size single- or poly-crystalline domains in a time period from days to weeks. Although these techniques are favorable for low volume, laboratory-scale production, their scaling-up to an industrial-scale mass-fabrication seems infeasible due to their tedious fabrication processes and incompatibility to the wafer-scale batch microfabrication widely used by the semiconductor industry. In addition, these methods lead to either nonuniform or noncontrollable crystalline thickness over large-area.

These restrictions also greatly impact the mass-fabrication and practical applications of another two types of technologically

* To whom correspondence should be addressed. Current address: Department of Chemical Engineering, Princeton University, Princeton, New Jersey 08544.

(1) Pieranski, P. *Contemp. Phys.* **1983**, *24*, 25–73.
(2) Xia, Y. N.; Gates, B.; Yin, Y. D.; Lu, Y. *Adv. Mater.* **2000**, *12*, 693–713.
(3) Weissman, J. M.; Sunkara, H. B.; Tse, A. S.; Asher, S. A. *Science* **1996**, *274*, 959–960.
(4) Kamenetzky, E. A.; Magliocco, L. G.; Panzer, H. P. *Science* **1994**, *263*, 207–210.
(5) Holtz, J. H.; Asher, S. A. *Nature* **1997**, *389*, 829–832.
(6) Asher, S. A.; Alexeev, V. L.; Goponenko, A. V.; Sharma, A. C.; Lednev, I. K.; Wilcox, C. S.; Finegold, D. N. *J. Am. Chem. Soc.* **2003**, *125*, 3322–3329.
(7) Velev, O. D.; Kaler, E. W. *Langmuir* **1999**, *15*, 3693–3698.
(8) Sharma, A. C.; Jana, T.; Kesavamoorthy, R.; Shi, L. J.; Virji, M. A.; Finegold, D. N.; Asher, S. A. *J. Am. Chem. Soc.* **2004**, *126*, 2971–2977.
(9) Sun, S. H.; Murray, C. B.; Weller, D.; Folks, L.; Moser, A. *Science* **2000**, *287*, 1989–1992.
(10) Siwick, B. J.; Kalinina, O.; Kumacheva, E.; Miller, R. J. D.; Noolandi, J. *J. Appl. Phys.* **2001**, *90*, 5328–5334.
(11) Pham, H. H.; Gourevich, I.; Oh, J. K.; Jonkman, J. E. N.; Kumacheva, E. *Adv. Mater.* **2004**, *16*, 516–520.
(12) Pusey, P. N.; Vanmegen, W. *Nature* **1986**, *320*, 340–342.
(13) Zhu, J. X.; Li, M.; Rogers, R.; Meyer, W.; Ottewill, R. H.; Russell, W. B.; Chaikin, P. M. *Nature* **1997**, *387*, 883–885.
(14) Ackerson, B. J.; Clark, N. A. *Phys. Rev. Lett.* **1981**, *46*, 123–126.
(15) Vlasov, Y. A.; Bo, X. Z.; Sturm, J. C.; Norris, D. J. *Nature* **2001**, *414*, 289–293.
(16) Blanco, A.; Chomski, E.; Grabtchak, S.; Ibisate, M.; John, S.; Leonard, S. W.; Lopez, C.; Meseguer, F.; Miguez, H.; Mondia, J. P.; Ozin, G. A.; Toader, O.; van Driel, H. M. *Nature* **2000**, *405*, 437–440.
(17) Wijnhoven, J.; Vos, W. L. *Science* **1998**, *281*, 802–804.
(18) Mayoral, R.; Requena, J.; Moya, J. S.; Lopez, C.; Cintas, A.; Miguez, H.; Meseguer, F.; Vazquez, L.; Holgado, M.; Blanco, A. *Adv. Mater.* **1997**, *9*, 257-&.
(19) Jethmalani, J. M.; Sunkara, H. B.; Ford, W. T.; Willoughby, S. L.; Ackerson, B. J. *Langmuir* **1997**, *13*, 2633–2639.
(20) Jethmalani, J. M.; Ford, W. T. *Chem. Mater.* **1996**, *8*, 2138–2146.
(21) van Blaaderen, A.; Ruel, R.; Wiltzius, P. *Nature* **1997**, *385*, 321–324.
(22) Ozin, G. A.; Yang, S. M. *Adv. Funct. Mater.* **2001**, *11*, 95–104.
(23) Park, S. H.; Xia, Y. N. *Langmuir* **1999**, *15*, 266–273.
(24) Jiang, P.; Bertone, J. F.; Hwang, K. S.; Colvin, V. L. *Chem. Mater.* **1999**, *11*, 2132–2140.
(25) Wong, S.; Kitaev, V.; Ozin, G. A. *J. Am. Chem. Soc.* **2003**, *125*, 15589–15598.
(26) Trau, M.; Saville, D. A.; Aksay, I. A. *Science* **1996**, *272*, 706–709.
(27) Hayward, R. C.; Saville, D. A.; Aksay, I. A. *Nature* **2000**, *404*, 56–59.

important materials—macroporous polymers and polymeric nanocomposites, as most of their fabrication methods involve the preformation of colloidal crystals as structural scaffolds.[28,29] Spontaneously organized colloidal crystals have been widely used as 3D templates for the construction of macroporous materials—so-called "inverted opals". In this approach, the voids between colloidal spheres are infiltrated with another material, such as metals,[30−33] semiconductors,[15,16,34,35] ceramics,[36−39] and polymers,[28,40−43] subsequent removal of the template by either wet etching or thermal decomposition leads to the formation of 3D ordered air cavities inside the void-filling materials. For example, macroporous polymers with crystalline arrays of voids have been fabricated by infiltrating and polymerizing monomers within preformed colloidal crystal templates.[28,40−43] Although the "breath figures" induced thermocapillary convective provides a much faster means in creating macroporous polymers,[44,45] the perfect periodic domain ordering can only be achieved over tens-of-micrometer-scale area, in comparison with centimeter-size domains in colloidal-crystal-templated samples. These highly ordered polymeric replicas with interconnected voids have successfully been demonstrated as separation media for macromolecules and DNA separation,[46,47] biosensors,[48] and "lost-wax" scaffolds for building complex colloids and colloidal crystals.[49,50] They are also promising candidates for low-*k* materials to reduce signal delay and cross-talk in interconnects within integrated circuits.[51]

Polymer-embedded colloidal crystals, or 3D ordered polymeric nanocomposites, have also found important technological applications ranging from photonic papers[52,53] to ultrahigh-density optical recording materials.[10,11] But, current self-assemblies based on electrostatic repulsion,[3,19] hybrid core−shell approach[54] and monomer infiltration of preformed colloidal crystals[52] are either difficult in controlling the final crystal thickness or tedious in forming a large-area sample. In practical, it is highly desirable to develop a technique that enables the mass-fabrication of large-area, planar samples with controllable thickness.

Herein, we describe a versatile spin-coating procedure that enables the rapid formation of 3D ordered silica colloidal crystals, macroporous polymers and polymeric nanocomposites. Wafer-scale samples, that are at least 1 order of magnitude larger than current available ones, can be routinely fabricated in minutes. The resultant planar samples have highly uniform thickness, which can be easily adjusted by changing the spin speed and time. We also show that patterns with micrometer-scale resolution can be created using standard semiconductor microfabrication techniques for potential device applications. Optical transmission studies of the 3D ordered structures illustrate the existence of optical stop bands, in which strong diffraction effects limit the optical transmission of the films.

Experimental Section

Materials and Substrates. All solvents and chemicals are of reagent quality and are used without further purification. Ethanol (200 proof) is obtained from Pharmaco Products. Ethoxylated trimethylolpropane triacrylate monomer (ETPTA, MW 428, viscosity 60 cps, SR 454) is purchased from Sartomer. The photoinitiator, Darocur 1173 (2-hydroxy-2-methyl-1-phenyl-1-propanone), is obtained from Ciba-Geigy. The silicon wafer primer, 3-acryloxypropyl trichlorosilane (APTCS), is purchased from United Chemical Technologies. Tetrabutylammonium chloride is purchased from Aldrich. Silicon wafers (test grade, n or p type, 600 nm thermal oxide layer, Wafernet, San Jose, CA) are cleaned in a "Piranha" solution (a 3:1 mixture of concentrated sulfuric acid with 30% hydrogen peroxide) for half an hour, rinsed with Milli-Q water (18.2 MΩ cm^{-1}), and dried in a stream of nitrogen. The cleaned silicon wafers are then primed by swabbing APTCS on the wafer surfaces using cleanroom Q-tips, rinsed with 200-proof ethanol twice, and baked on a hot plate at 110 °C for two minutes.

Instrumentation. Scanning electron microscopy and EDAX are carried out on a LEO 982 FEG-SEM. A Thermdyne Maxi Solution Mixer (type 37600) is used to disperse silica colloids in ETPTA monomers. A standard spin coater (CEE Model 100, Brewer Science) is used to spin-coat silica-ETPTA dispersion onto different substrates. The polymerization of ETPTA monomers is carried out on a commercial Tamarack exposure unit operating at 23.5 mJ/cm². An interference-based Film Thickness Measurement System (F20, Filmetrics) is used to measure the polymerized nanocomposite film thickness. Photolithography is carried out on a Karl Suss MA6 mask aligner. An oxygen plasma etcher (Quartz Series, Anatech) is used to remove polymerized ETPTA for releasing colloidal crystals and a reactive ion etcher (RIE, PlasmaTherm 790, Unaxis) is used to pattern nanocomposite films. Transmission spectra are obtained by using a Cary 5 UV−vis−NIR spectrometer.

Preparation of Colloidal Dispersions. The synthesis, purification and volume fraction determination of highly uniform silica microspheres with less than 5% diameter variation in 200-proof ethanol are performed according to ref 24. After complete centrifugation of the calculated amount of purified silica solution and discarding of the supernatant solvent, silica colloids are re-dispersed in ETPTA monomers using a Thermdyne Maxi Solution Mixer. 1% (weight) Darocur 1173 is added as the photoinitiator. The final particle volume fraction is about 19.8%. After filtration through a 5 *μ*m syringe filter (Millipore) to remove any large particles, the transparent and viscous solution is stored in an open vial for overnight to allow any residual ethanol to evaporate.

Spin-Coating of Colloidal Dispersions and Photopolymerization. All of the following experiments are done in a class 100 cleanroom,

(28) Jiang, P.; Hwang, K. S.; Mittleman, D. M.; Bertone, J. F.; Colvin, V. L. *J. Am. Chem. Soc.* **1999**, *121*, 11630−11637.
(29) Kumacheva, E.; Kalinina, O.; Lilge, L. *Adv. Mater.* **1999**, *11*, 231−234.
(30) Velev, O. D.; Tessier, P. M.; Lenhoff, A. M.; Kaler, E. W. *Nature* **1999**, *401*, 548−548.
(31) Jiang, P.; Cizeron, J.; Bertone, J. F.; Colvin, V. L. *J. Am. Chem. Soc.* **1999**, *121*, 7957−7958.
(32) Egan, G. L.; Yu, J. S.; Kim, C. H.; Lee, S. J.; Schaak, R. E.; Mallouk, T. E. *Adv. Mater.* **2000**, *12*, 1040−1042.
(33) Li, F.; Xu, L. B.; Zhou, W. L.; He, J. B.; Baughman, R. H.; Zakhidov, A. A.; Wiley: J. B. *Adv. Mater.* **2002**, *14*, 1528−1531.
(34) Braun, P. V.; Wiltzius, P. *Nature* **1999**, *402*, 603−604.
(35) Vlasov, Y. A.; Yao, N.; Norris, D. J. *Adv. Mater.* **1999**, *11*, 165−169.
(36) Velev, O. D.; Jede, T. A.; Lobo, R. F.; Lenhoff, A. M. *Nature* **1997**, *389*, 447−448.
(37) Holland, B. T.; Blanford, C. F.; Stein, A. *Science* **1998**, *281*, 538−540.
(38) Stein, A.; Schroden, R. C. *Curr. Opin. Solid St. Mater. Sci.* **2001**, *5*, 553−564.
(39) Zakhidov, A. A.; Baughman, R. H.; Iqbal, Z.; Cui, C. X.; Khayrullin, I.; Dantas, S. O.; Marti, I.; Ralchenko, V. G. *Science* **1998**, *282*, 897−901.
(40) Park, S. H.; Xia, Y. N. *Adv. Mater.* **1998**, *10*, 1045−1048.
(41) Johnson, S. A.; Ollivier, P. J.; Mallouk, T. E. *Science* **1999**, *283*, 963−965.
(42) Deutsch, M.; Vlasov, Y. A.; Norris, D. J. *Adv. Mater.* **2000**, *12*, 1176−1180.
(43) Lee, W.; Pruzinsky, S. A.; Braun, P. V. *Adv. Mater.* **2002**, *14*, 271.
(44) Srinivasarao, M.; Collings, D.; Philips, A.; Patel, S. *Science* **2001**, *292*, 79−83.
(45) Song, L.; Bly, R. K.; Wilson, J. N.; Bakbak, S.; Park, J. O.; Srinivasarao, M.; Bunz, U. H. F. *Adv. Mater.* **2004**, *16*, 115−118.
(46) Liu, L.; Li, P. S.; Asher, S. A. *Nature* **1999**, *397*, 141−144.
(47) Nykypanchuk, D.; Strey, H. H.; Hoagland, D. A. *Science* **2002**, *297*, 987−990.
(48) Qian, W. P.; Gu, Z. Z.; Fujishima, A.; Sato, O. *Langmuir* **2002**, *18*, 4526−4529.
(49) Jiang, P.; Bertone, J. F.; Colvin, V. L. *Science* **2001**, *291*, 453−457.
(50) Yang, S. M.; Coombs, N.; Ozin, G. A. *Adv. Mater.* **2000**, *12*, 1940−1944.
(51) Miller, R. D. *Science* **1999**, *286*, 421−422.
(52) Fudouzi, H.; Xia, Y. N. *Langmuir* **2003**, *19*, 9653−9660.
(53) Arsenault, A. C.; Miguez, H.; Kitaev, V.; Ozin, G. A.; Manners, I. *Adv. Mater.* **2003**, *15*, 503−507.
(54) Kalinina, O.; Kumacheva, E. *Macromolecules* **1999**, *32*, 4122−4129.

though this is not a definite requirement. 600 μL of above silica-ETPTA solution is dispensed on a substrate. After tilting and rotating the substrate to spread the solution to achieve full wafer coverage, the wafer is spin-coated at 200 rpm on a standard spin-coater for one minute. Six-arm diffraction star is formed in about 30 s. The wafer is then quickly accelerated (2000 rpm/sec) to the desired spin speed and continues to spin for the specific time to achieve the target thickness. Acetone is used for wafer edge bead removal. After spin-coating, the wafer is transferred to a vacuum chamber equipped with a quartz window, and pumped down to 0.1–1.0 Torr in 30 s. After back-filling with nitrogen for 90 s, the monomer is photopolymerized using a Tamarack exposure unit operating at 23.5 mJ/cm^2 for 212 s to obtain overall exposure dose of 5 J/cm^2.

Controlling Film Thickness by Spin-Coating Speed and Time. The polymerized nanocomposite film thickness is measured using an interference-based Film Thickness Measurement System (F20, Filmetrics). An average refractive index of 1.433 of the nanocomposite film is obtained from six samples (325 nm colloids) of different thickness using a Metricon 2010 refractive index measurement system and is used for the film thickness measurement. For determining the relationship of the film thickness with the final spin speed, six four-inch samples (325 nm diameter) are prepared at different spin speed, 300, 600, 1200, 2000, 4000, and 6000 rpm, for constant spin time, 120 s. Over 40 random spots on the four-inch samples are measured, providing average film thickness. For determining the relationship of the film thickness with the final spin time, six 4-inch samples (325 nm diameter) are prepared at different spin time, 30, 90, 120, 240, 480, and 960 s, for constant spin speed, 600 rpm.

Selective Removal of ETPTA Polymer Matrix and Silica Spheres. An oxygen plasma etcher (Quartz Series, Anatech) operated at 1 Torr oxygen pressure, 450 sccm oxygen flow rate and 500 W, is used to remove ETPTA polymer matrix for releasing embedded colloidal crystals. It takes about 5–6 min for complete removal of the polymer matrix of a 30 μm thick sample. To remove silica spheres for making macroporous polymers, the same plasma etcher is used at the same conditions for only 10 s to partially remove ETPTA polymer layer on the surface and to expose the top layer of silica spheres. This can greatly reduce the etching time of silica spheres from overnight without plasma etching to less than 10 min for a ~30 μm thick sample, while the ordering and porosity of the resulting macroporous polymers are not affected. 2% hydrofluoric acid aqueous solution is used to remove silica templates.

Proximity Photolithography and Reactive Ion Etch (RIE). For proximity photolithography patterning, the spin-coated wet colloidal crystal-monomer film is covered with a photomask with pieces of tungsten wires (GoodFellow, Cambridge) used as spacers for separating the photomask and the monomer-coated wafer. Tungsten wires of different diameters are chosen to make the proximity gap as small as possible, typically less than five-micron. After exposure to UV radiation at 23.5 mJ/cm^2 for four seconds, the un-exposed monomer and silica colloids are removed by acetone rinse. The wafer is then flood-exposed to 5 J/cm^2 dose for complete polymerization. For RIE patterning, 300-nm-thick aluminum (DC magnetron sputtering deposited using a Perkin-Elmer 2400 Metallization System) is photolithographically patterned using conventional photoresist and wet etched to open etching windows in the aluminum layer. An oxygen reactive ion etcher (PlasmaTherm 790, Unaxis) operated at 30 mTorr oxygen pressure, 50 sccm flow rate and 500 W power, is then used to remove ETPTA underneath the etching windows. It takes about 5 min for complete removal of uncovered ETPTA of a 30-micron-thick sample. The exposed silica spheres can then be removed by 1% hydrofluoric acid rinse for 40 s.

Sample Characterization. Scanning electron microscopy and EDAX are carried out on a LEO 982 FEG-SEM. A thin layer of gold is sputtered onto the samples prior to imaging. The optical properties of the resultant samples are evaluated by measuring their transmission spectra at normal incidence, using a Cary 5 UV–vis–NIR spectrometer.

The optical samples were prepared on glass slides instead of on silicon wafers for transmission measurement.

Supporting Video Clip. Real time video clip of shear-induced crystallization during spin coating of 325 nm silica-ETPTA dispersion is obtained with a Panasonic PV-DV 951 digital camcorder. After swirling the dispersion to cover the four-inch silicon wafer with iridescent polycrystalline, the sample is accelerated to 200 rpm (100 rpm/s acceleration rate) for one minute and then spun at 300 rpm for another one minute, followed by final spin at 6000 rpm (2000 rpm/s acceleration rate) for one minute. The original three-minute clip is trimmed to 56 s to save memory. The edited clip includes the first thirty seconds of the original video, illustrating the ready formation of six-arm diffraction star, followed by a fifteen-second clip of the transition from 200 to 300 rpm and a seven-second clip of the acceleration from 300 to 6000 rpm, and then the final four seconds spinning at 6000 rpm. A fiber optic illuminator (Model 190, Fiber-Lite) is used to provide a collimated light beam (~45° to the surface normal).

Results and Discussion

Spin coating of volatile colloidal dispersions has been widely used in preparing colloidal masks for "natural lithography".[55] However, only thin-layer samples (typically 1–2 layers) with centimeter-sized area can be created and the resultant polycrystalline samples have poor crystalline qualities. Well-ordered multilayer colloidal crystals have been made by spin-coating of submicron spheres within pyramid-shaped etch pits.[22] A combination technique of centrifugation and spin-coating has been developed to assemble centimeter-sized colloidal crystals with tapered thickness profile.[56] We disperse uniform silica colloids in viscous and nonvolatile monomers, ethoxylated trimethylolpropane triacrylate (ETPTA), with 1% Darocur 1173 as photoinitiator to make a final particle volume fraction of 19.8%. There is no need for extra solvent or surface modification of the silica spheres. The resultant transparent dispersion is stable for at least six months for small spheres (<400 nm); whereas for larger spheres, the precipitation of particles reduces the solution stability to 1 to 3 months, but agitation can easily re-disperse the sediment. We attribute the colloidal stability to the index matching between silica colloids (1.42)[57] and ETPTA monomers (1.4689), which reduces the attractive van der Waals forces between spheres.[58] Although we only use silica-ETPTA dispersions here, surface modification of silica colloids with organosilane can greatly extend the availability of stable colloid/monomer dispersions, which can also be used in similar spin-coating processes for inducing colloidal crystallization.[59]

The silica-ETPTA dispersion is dispensed on a variety of substrates, such as silicon wafers, glass slides, lithium niobate wafers and PMMA plates, and spin-coated on a standard spin coater. Under white light illumination, a strong monochromatic diffraction star with six arms (Figure 1) gradually replaces the iridescent polycrystalline appearance formed prior to spin coating, in about 30 s (see the video clip of the Supporting Information). The adjacent arms of the diffraction star form exact 60° angles, indicating the formation of hexagonally packed

(55) Deckman, H. W.; Dunsmuir, J. H. *Appl. Phys. Lett.* **1982**, *41*, 377–379.
(56) Xu, Y.; Schneider, G. J.; Wetzel, E. D.; Prather, D. W. *Proc. SPIE Int. Soc. Opt. Eng.* **2003**, *5183*, 16–24.
(57) Bogush, G. H.; Tracy, M. A.; Zukoski, C. F. *J. Non-Cryst. Solids* **1988**, *104*, 95–106.
(58) Russel, W. B.; Saville, D. A.; Schowalter, W. R. *Colloidal Dispersions*; Cambridge University Press: Cambridge, 1989.
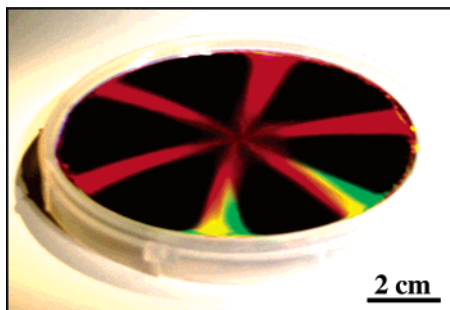(59) Philipse, A. P.; Vrij, A. *J. Colloid Interface Sci.* **1989**, *128*, 121–136.

Figure 1. Photograph of a 3D ordered nanocomposite film on a 4-inch silicon wafer illuminated with white light. The sample is made from 325 nm diameter colloidal spheres and spin-coated at 600 rpm for 120 s.
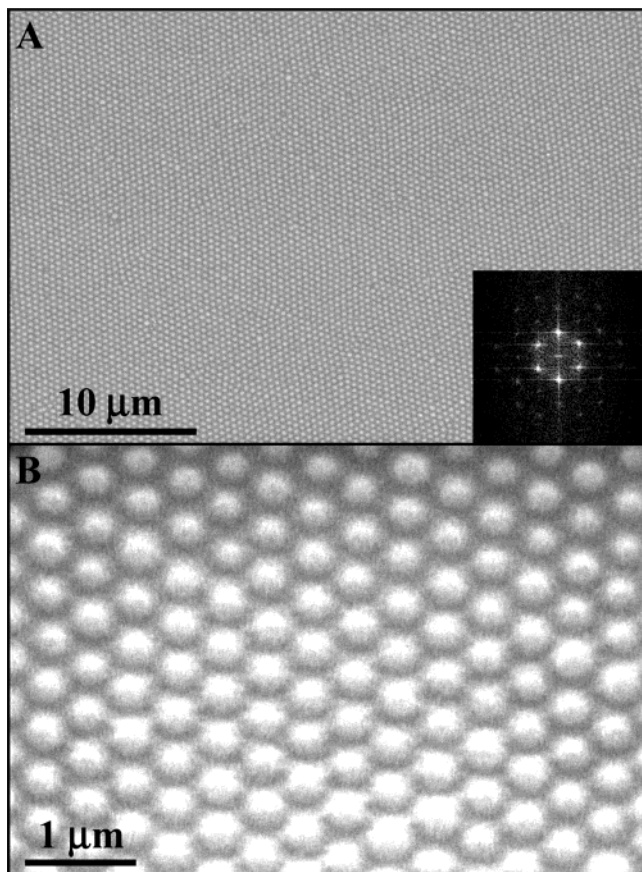

Figure 2. Typical scanning electron microscope (SEM) images of a spin-coated colloidal crystal-polymer nanocomposite film. (A) Top-view image of the sample in Figure 1. The inset showing a Fourier transform of a 40 × 40 μm region. (B) Higher magnification SEM image of the same sample.

Figure 3. Scanning electron microscope images and Fourier transforms (FFT) of four regions of a 4-inch nanocomposite film spin-coated using 325 nm diameter colloids. These images are part of a series taken every 1 cm over the sample surface; they represent four spots that are 4 cm away from the center of the sample and rotate from top (A) to right (B) to bottom (C) to left (D). The four parallel dashed lines indicate one reference direction. The largest deviation from this orientation is ~10° for these images and all intermediate images.

Figure 4. Typical side-view SEM images of spin-coated nanocomposite films with different thickness. (A) A 2-layer sample coated at 6000-rm for 900 s. (B) A 5-layer sample coated at 6000-rpm for 170 s. (C) A 41-layer sample coated at 600-rpm for 120 s 325 nm diameter colloids are used for all cases.

spheres parallel to the wafer surface.[1,60] As the packing assumed by the spheres during spin coating is stable and the fluid surrounding the spheres is viscous, the aligned crystals persist after spinning ceases. The monomers are then polymerized by exposure to ultraviolet radiation.

The as-synthesized colloidal crystal-polymer nanocomposite film exhibits bright monochromatic diffraction (Figure 1). When the incident angle of the illuminating white light is fixed while the wafer is rotating, the six arms of the diffraction star are stationary (see the video clip), indicating globally even distribution of hexagonally packed spheres. Multiple reflected colors of Figure 1 are caused by other orders of Bragg diffraction. A
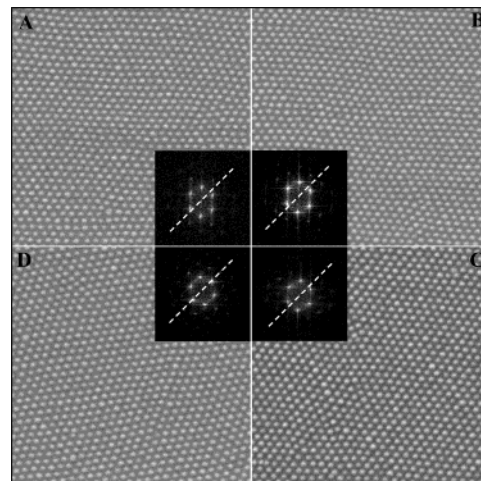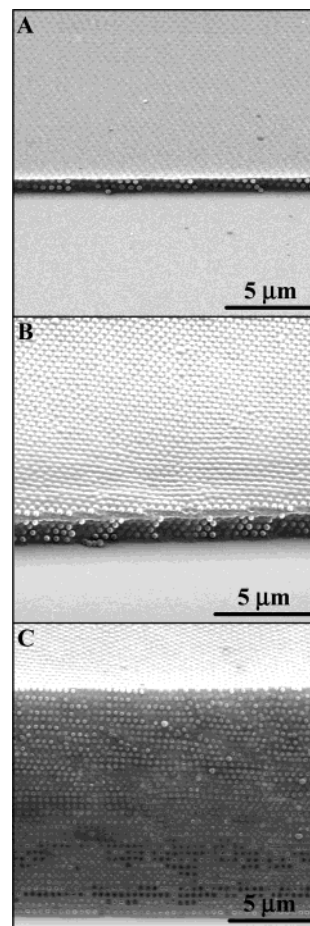
scanning electron microscope (SEM) image (Figure 2A) and its Fourier transform (FFT, inset of Figure 2A) demonstrate the

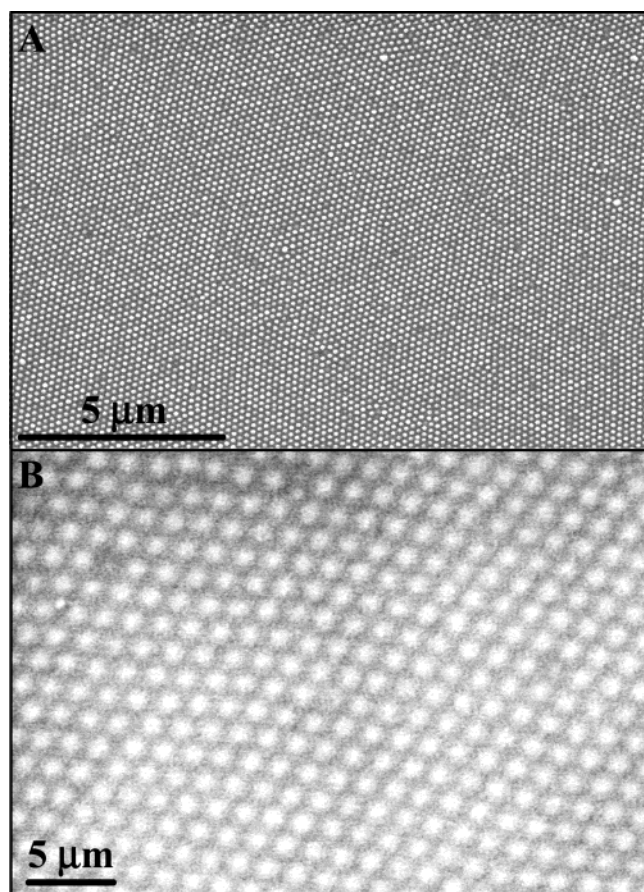(60) Hoffman, R. L. *Trans. Soc. Rheol.* **1972**, *16*, 155−165.

Figure 5. Typical top-view SEM images of spin-coated nanocomposite films with different sphere sizes. (A) A sample made from 130 nm diameter spheres and coated at 600 rpm for 120 s. (B) A sample made from 1320 nm diameter spheres and coated at 600 rpm for 120 s.

highly ordered structures with hexagonal packing on the film surface. At higher magnification, another interesting feature is evident, i.e., the spheres of the top layer are not touching each other, but exhibit center-to-center distance around 1.41D (Figure 2B), where D is the diameter of colloids. The non-close-packing of colloids is more apparent after the polymer matrix been selectively removed by oxygen plasma etching (Figure 7C). Extensive SEM and Fourier transform (FFT) studies over a 4-inch sample reveal that the change of the crystallographic orientation is less than 10° (Figure 3). The ordering perpendicular to the regularly arranged top plane is apparent in the cross-sectional images (Figure 4A, B, and C). But, these perspective views cannot determine the real crystalline structure, which is still under investigation.

The spin-coating technique described here has a number of advantages over previous self-assemblies. First of all, it is rapid and highly manufacturable. Four-inch-diameter planar crystal (81-cm^2, Figure 1), which is an order of magnitude larger than currently available ones, can be routinely made in minutes; whereas early methods take days or even weeks to produce a centimeter-size crystal.[18,24] The wide particle diameter range achievable with this technique is another advantage over previous methods, as quick gravitational sedimentation of large silica spheres (>400 nm) causes serious problems in making high-quality crystals.[15,24,25] From the well-known sedimentation equation,[58] $v = (2/9) (R_s^2 \Delta \rho g/\eta)$, ($R_s$ is the sphere radius, $\Delta \rho$ is the density difference between silica and solvent, η is the
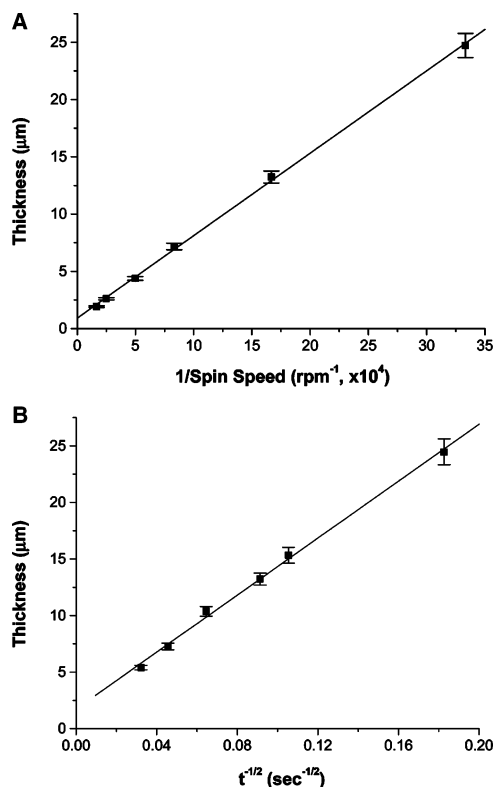
Figure 6. Precise control of the crystal thickness. (A) Linear relationship of the crystal thickness vs the inverse of the spin speed at constant coating time, 120 s. (B) Film thickness vs the inverse of the square root of spin time at constant spin speed, 600 rpm. 325 nm diameter colloids are used for all cases.

solvent viscosity), we can estimate that the sedimentation velocity of silica in ETPTA is about 70-times slower than that in water. Given the short spin-coating and photopolymerization time (in minutes), the formidable challenge of sedimentation can be completely avoided. Using this spin-coating technique, monodisperse silica colloids with a wide diameter range from 100 nm to 2 μm can be cast to form 3D ordered nanocomposite films. Two samples made from 130 nm (Figure 5A) and 1320 nm (Figure 5B) diameter colloids show similar long-range ordering and center-to-center distance (around 1.41D) as those of 325 nm spheres (Figure 2).

Crystalline thickness is another important parameter in determining the quality of resultant crystals. Highly uniform and tunable film thickness over a large area is much favored for the simultaneous production of multiple devices on a single substrate. Spin-coating is a well-established technique for reproducibly forming large-area, highly uniform thickness films from viscous solutions.[61] Our spin-coated nanocomposite films exhibit excellent thickness uniformity with variation within a 4-inch-diameter wafer of less than 4%, as determined by a Film Thickness Measurement System (F20, Filmetrics). The film thickness (from monolayer to over one hundred colloidal layers) can be controlled easily by changing the spin speed and time (Figure 6). It is inversely proportional to the final spin speed (Figure 6A) and the square root of the final spin time (Figure 6B). This agrees well with the model of spin coating of solvent-free liquids,[62] which predicts $H \approx (A/\omega \sqrt{t})$, where H is the

(61) Madou, M. J. *Fundamentals of Microfabrication: The Science of Miniaturization*, 2nd ed.; CRC Press: Boca Raton, FL, 2002.
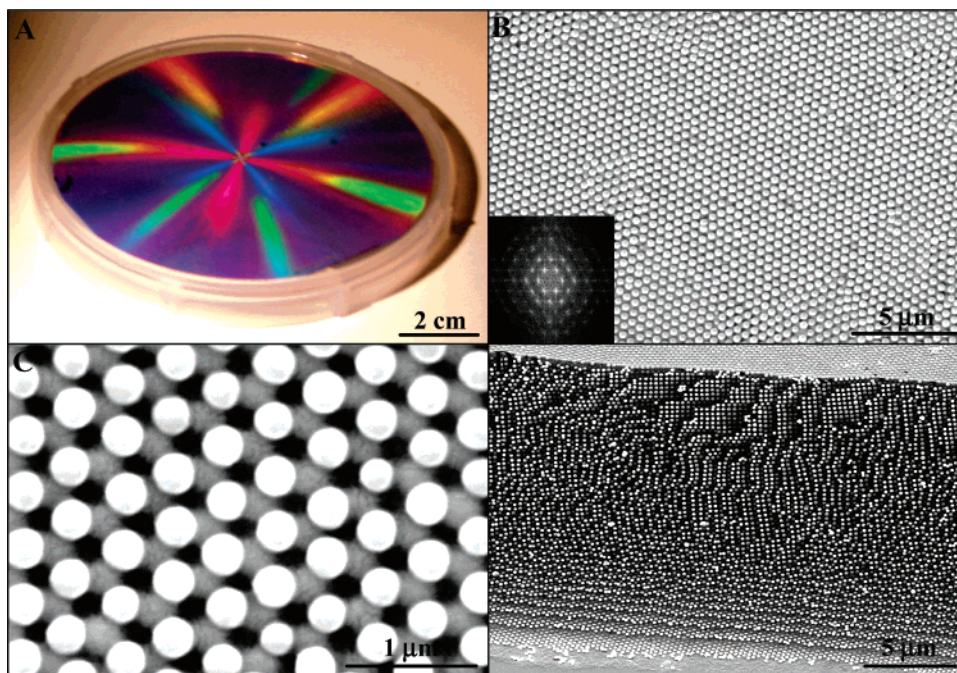(62) Middleman, S. *J. Appl. Phys.* **1987**, *62*, 2530–2532.

Figure 7. Formation of wafer-scale colloidal crystals by selective removal of polymer matrix. (A) Photo of a released colloidal crystal on a 4-inch silicon wafer. (B) Typical SEM image and its Fourier transform (inset) of the above sample. (C) Higher magnification image. (D) Cross-sectional SEM image.
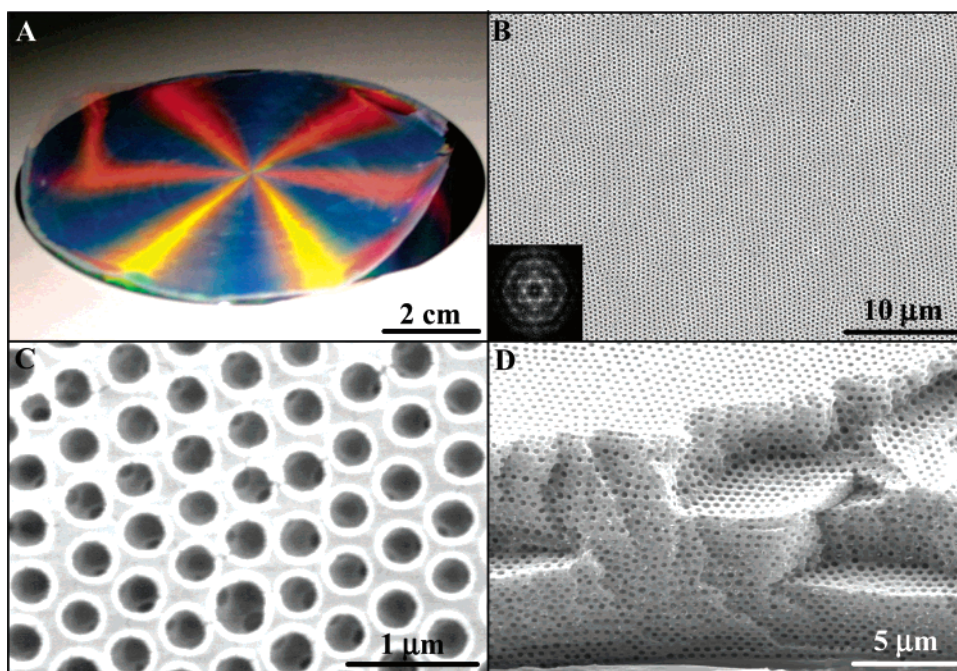

Figure 8. Self-standing macroporous polymer replica after removal of silica spheres by wet etching. (A) Photograph of a film placed on a 4-inch silicon wafer illuminated with white light. The wafer is only used for providing a dark background and a size reference. 325 nm silica sphere dispersion is spin-coated at 600 rpm for 270 s to make the template. (B) Top-view SEM image and its Fourier transform (inset) of the sample in (A). (C) Higher magnification image showing interconnected inner pores. (D) Side-view SEM image.

film thickness, A is a constant determined by the viscosity and density of the solution, ω and t are the final spin speed and time. From Figure 6, we get $A \approx 97800$ in the above approximation equation, where H is in microns, ω is in rpm and t is in seconds. The nanocomposite film thickness determines the number of layers of the resultant colloidal crystals and macroporous polymers, illustrated by three crystals of 2 colloidal layers (Figure 4A), 5 layers (Figure 4B) and 41 layers (Figure 4C) made at different spin-coating conditions. The resultant 3D ordered planar nanocomposites with well-controlled

thickness are highly desirable for the development of ultrahigh-density magnetic and optical recording materials.[9−11]

Besides providing a versatile route to create 3D ordered nanocomposites, this technique's major merit is in its ability to mass-fabricate planar colloidal crystals and macroporous polymers. Due to their substantial difference in chemical properties, ETPTA and silica can each be selectively removed without disturbing the structure of the other, resulting in the formation of colloidal crystals and macroporous polymers, respectively. Oxygen plasma etching is a better method than calcination in
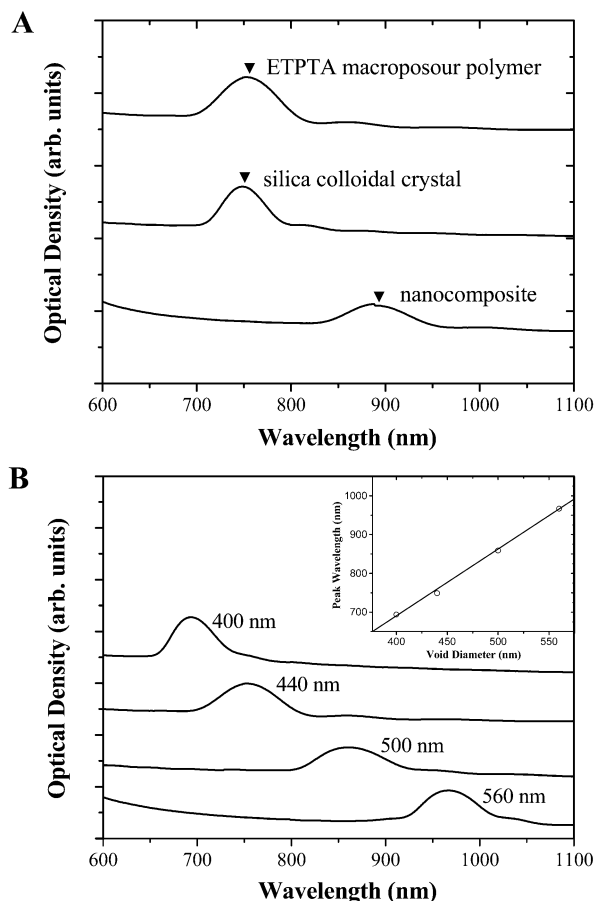
Figure 9. Normal incidence transmission spectra (optical density). (A) Spectra of an ETPTA-silica colloidal crystal nanocomposite, a respective macroporous ETPTA polymer film and a respective silica colloidal crystal with 440 nm diameter and 15 colloidal layers. These curves have been vertically offset for clarity. The arrows indicate the expected positions of the peaks for each sample, calculated using Bragg's law at normal incidence. (B) Spectra of macroposous ETPTA samples with different void diameters, determined using SEM analysis. The inset shows wavelength at which the optical transmission spectrum peaks as a function of void diameter. The open circles are experimental points measured at normal incidence. The solid curve shows the calculated value for the inverted macroporous structures.

removing ETPTA polymer matrix, as it hardly affects the silica spheres and no defects, such as cracks, are introduced. The resultant planar colloidal crystal exhibits stronger Bragg diffraction (Figure 7A) than nanocomposite due to the increase in refractive index contrast when air replaces the polymer fraction. An SEM image (Figure 7B) and its Fourier transform (inset of Figure 7B) reveal the expected hexagonal arrangement of spheres. Similar to the original nanocomposites, intralayer silica spheres keep their initial $1.41D$ center-to-center distance (Figure 7C). It is also interesting to notice that spheres of the top layer only fill in the triangularly arranged crevices made by the nontouching spheres of the second layer (Figure 7C). Underneath, hexagonally packed layers throughout the film thickness exhibit similar intralayer nonclose-packing and good registry between neighboring layers (Figure 7D).

Conversely, embedded silica spheres can be selectively removed by hydrofluoric acid wash to make large-area, flexible and free-standing macroporous polymers. The bright iridescent colors of such a film (Figure 8A) are caused by Bragg diffraction of visible light from 3D ordered air cavities, evidenced by top-
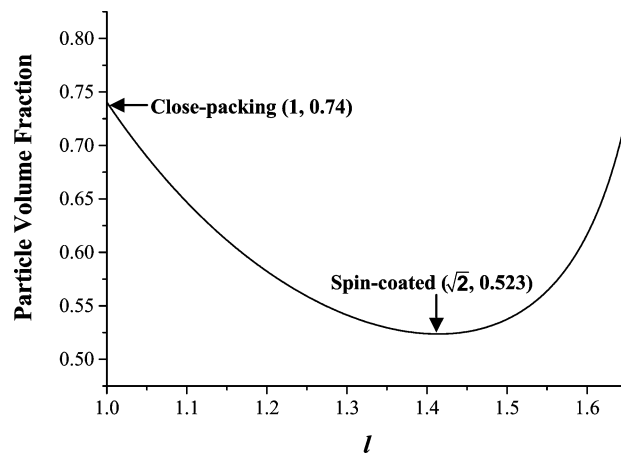
Figure 10. Relationship between particle volume fraction of possible crystals during vertical compressing vs the ratio, *l*, of in-plane particle center-to-center distance to the sphere diameter.

and side-view SEM images (Figure 8B and D) and Fourier transform (inset of Figure 8B). At higher magnification, the interconnecting inner pores, arising from the touching sites of silica spheres in the original nanocomposites, are obvious (Figure 8C). But, only 6 pores instead of $12^{16,28,34,39}$ are visible, because each inner silica sphere simply contacts with 3 upper-layer spheres and 3 bottom-layer spheres, not with the 6 neighboring spheres in the same plane (Figure 7C). The interconnected pores ensure the complete removal of silica templates in resultant macroporous polymers, confirmed by the absence of elemental silicon in the energy-dispersive X-ray analysis (EDAX). Such polymeric materials with ordered and interconnected pores are valuable as separation media for macromolecules and DNA separation,[46,47] biosensors[48] and low-*k* substrates.[51]

Above scanning electron microscope studies on the structures of spin-coated nanocomposite films and templated silica colloidal crystals and macroporous polymers indicate that in-plane neighboring spheres separate from each other by $\sim\sqrt{2}D$, whereas inter-plane neighboring spheres touch with each other; otherwise, the released colloidal crystal would collapse during plasma etching and the interconnecting pores in macroporous polymer would not form. By simple geometrical calculation, we found that the interlayer spacing is $\sqrt{2}/2D$ and the volume fraction of silica particles in the original nanocomposite film is only $\sim$53%. This unusual open crystalline structure is verified by optical characterization using visible-near-IR transmission at normal incidence. Figure 9A shows optical transmission spectra for a nanocomposite and respective macroporous ETPTA and silica colloidal crystal films made from 440 nm silica spheres. The spectra show strong peaks due to the Bragg diffraction of visible and near-IR light from the ordered structures. The peak height of the nanocomposite film is lower than that of silica colloidal crystal and macroporous ETPTA polymer due to smaller refractive index contrast.[63] The position of the diffraction peaks can be related to the sphere diameter and the effective refractive index of the medium using Bragg's law: at normal incidence (where $\sin\theta_{inc} = 1$), $\lambda_{peak} = 2n_{eff}d$, where *d* is the interlayer spacing. The effective refractive index of the medium is calculated using $n_{eff} = n_1f_1 + n_2f_2$, where n_1

(63) Bertone, J. F.; Jiang, P.; Hwang, K. S.; Mittleman, D. M.; Colvin, V. L. *Phys. Rev. Lett.* **1999**, *83*, 300−303.
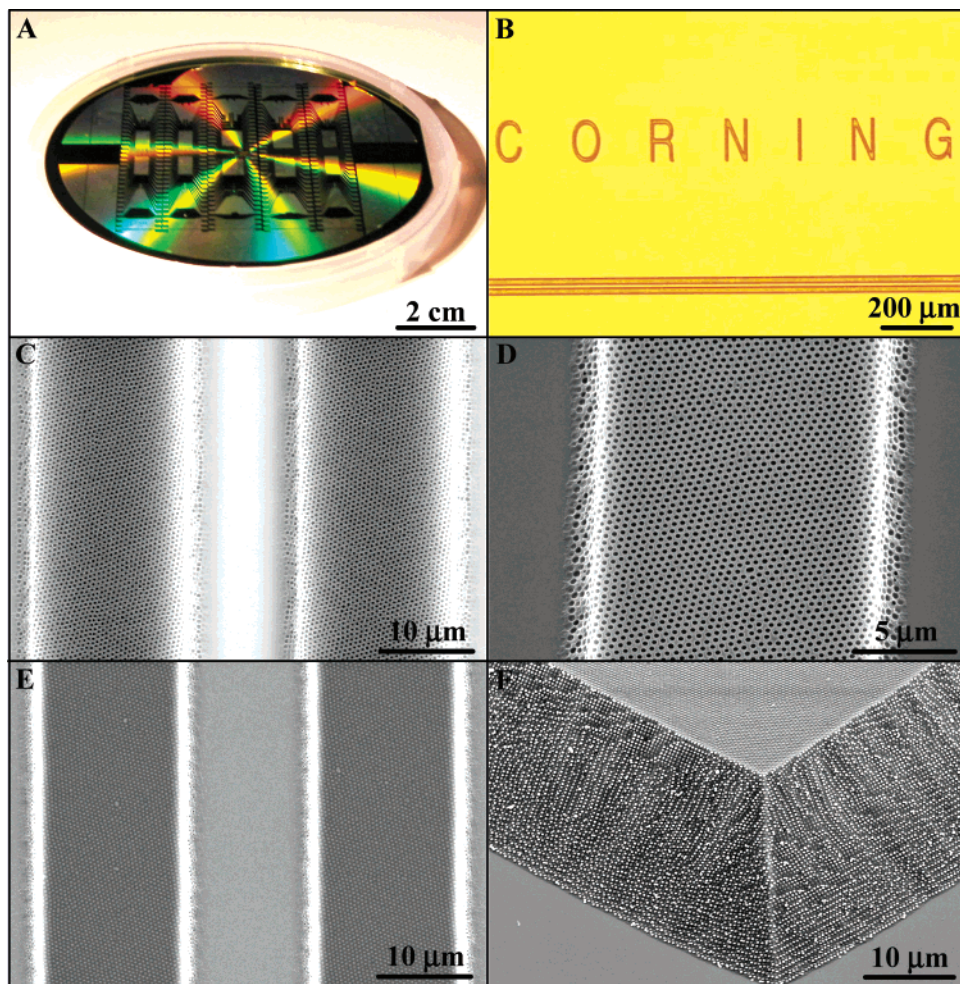
Figure 11. Making micro-patterns in layers of macroporous polymer and planar colloidal crystals by standard semiconductor microfabrication. (A) Photo of a patterned macroporous polymer film made by proximity photolithography. 325 nm silica dispersion is coated at 600 rpm for 60 s prior to lithography. (B) Optical microscopic image of fine features in (A) taken by a Nikon Optiphot 200C optical microscope. (C) Top-view SEM image of the parallel double lines in (B). (D) Higher magnification SEM image of a single line in (C). (E) Same sample as (D) prior to silica removal by wet etching. (F) Side-view SEM image of a patterned colloidal crystal film made by isotropic reactive ion etching. The nanocomposite is made from 325 nm diameter colloids and coated at 600 rpm for 120 s.

and n_2 are refractive index of the components and f_1 and f_2 are their corresponding volume fraction. For example, for ETPTA-silica nanocomposite, $n_{eff} = 1.42 \times 0.53 + 1.4689 \times 0.47 = 1.443$, which is very close to the measured effective refractive index (1.433) using a Metricon 2010 refractive index measurement system. The arrows that are shown in Figure 9A are peak positions predicted from the Bragg equation using sphere size as determined from SEM; agreement with experimental data is quite good. Figure 9B shows the optical transmission spectra for four macroporous ETPTA samples made from silica spheres ranging from 400 to 560 nm. Inset of Figure 9B shows the predicted peak position, λ_{peak}, versus void diameter; again the data is in good agreement with Bragg's law.

We attribute the colloidal crystallization by spin-coating to both shear induced ordering and subsequent monomer polymerization. Being a valuable model for probing the effect of shear flow on the generic properties of atomic systems, shear ordered colloidal crystallization has been extensively studied.[60,64-70] These studies have revealed a sliding layer structure at large

strain amplitudes and a twined fcc structure at small ones. In our spin-coating experiment, the typical shear rates are high ($>10^5$), resulting in a sliding layer mechanism, where 2D hexagonally packed colloidal layers are readily formed due to the coupling of the centrifugal ($\rho\omega^2 r$) and viscous ($-\eta(\partial^2 v/\partial^2 z)$) forces.[60] The interparticle electrostatic repulsion plays only a minor role due to the low dielectric constant of the ETPTA medium ($\sim$3 at optical frequency).[58] We also tested salt effect on the colloidal crystallization process during spin coating by adding 10^{-3} M tetrabutylammonium chloride to the silica-ETPTA dispersion (10% v/v 200-proof ethanol was added as cosolvent) to screen interparticle electrostatic repulsion and make silica colloids more "hard-sphere" like. The resultant spin-coated nanocomposite exhibits the same in-plane particle separation ($\sim$1.41D) and optical transmission spectrum as those samples made without the addition of salt, indicating minor contribution of the electrostatic force to the colloidal crystallization.

(64) Ackerson, B. J.; Clark, N. A. *Phys. Rev. A* **1984**, *30*, 906−918.
(65) Ackerson, B. J. *J. Phys. Condens. Mater.* **1990**, *2*, SA389−SA392.
(66) Chen, L. B.; Ackerson, B. J.; Zukoski, C. F. *J. Rheol.* **1994**, *38*, 193−216.
(67) Amos, R. M.; Rarity, J. G.; Tapster, P. R.; Shepherd, T. J.; Kitson, S. C. *Phys. Rev. E* **2000**, *61*, 2929−2935.
(68) Dux, C.; Versmold, H. *Phys. Rev. Lett.* **1997**, *78*, 1811−1814.
(69) Haw, M. D.; Poon, W. C. K.; Pusey, P. N. *Phys. Rev. E* **1998**, *57*, 6859−6864.
(70) Versmold, H. *Phys. Rev. Lett.* **1995**, *75*, 763−766.

Our experiment is different from previous shear-annealing studies as there is material spin-off during the spin-coating process. Colloids close to the wafer edges and surfaces experience the highest rotational velocities, thus are repelled from the wafer first. This can explain why we never observe monolayer steps on the film surface as the spin-off process occurs at the wafer edges and surfaces rather than at the top solution surface. To keep the continuity of the film, neighboring spheres move to the vacancies left by the repelled colloids, resulting in a convective radial particle flow, which leads to a pressure gradient exerted normal to the free film surface. It is believed that subsequent monomer photopolymerization plays another role in the formation of unusual open crystalline structure. Ellipsometry study (F20, Filmetrics) shows that ETPTA monomer undergoes ~4% volume shrinkage during polymerization. Due to the adhesion of ETPTA to the substrate, shrinkage mostly occurs in thickness direction as reported before,[71] resulting in additional normal pressure exerted on the stacked colloidal layers. By a simple geometrical calculation, the volume fraction (VF) of possible crystals during the vertical compressing can be related to the ratio, l, of in-plane particle center-to-center distance to the sphere diameter, as: $VF = (\pi/3l^2\sqrt{3-l^2})$. Figure 10 shows the relationship between the calculated volume fraction vs l. We found that the minimal volume fraction occurs at $l = \sqrt{2}$, which is corresponding well to the observed ~$1.41D$ in-plane particle separation (Figures 2, 5 and 7C). Therefore, we believe the normal pressures created by spin-coating and monomer polymerization squeeze the hexagonally arranged colloidal layers into each other, resulting in the formation of the unexpected non-close-packing structure, which is energetically favorable. Similar crystal structure tunability has recently been demonstrated by applying a vertical electric field in a colloidal suspension.[72] Although the underlying mechanism has yet to be fully understood, the spin-coating process provides a simple technique in creating wafer-scale colloidal crystals with low volume fraction, which are favorable for opening wider photonic band gaps.[73]

To make practical devices, patterning of as-synthesized nanocomposites, colloidal crystals, and macroporous polymers with micrometer regime resolution is important. The planar configuration, globally uniform thickness and wafer supported structure of these samples allow the simultaneous construction of multiple micrometer-dimensioned patterns using two standard semiconductor microfabrication techniques, proximity photolithography and reactive ion etching (RIE). A patterned macroporous polymer film (Figure 11A) made by proximity photolithography, shows iridescent colors, indicating the preservation of the ordered structures throughout the patterning and etching processes. To prevent the polymer from peeling off the substrate during wet etching, silicon wafers with native oxide layers are primed using 3-acryloxypropyl trichlorosilane (APTCS), which provides both protection of the oxide layers and covalent bond linkage between the wafer and ETPTA polymer. Under an optical microscope, the well-defined features of the sample are obvious (Figure 11B). When viewed at higher magnification under SEM, the regularly arranged air cavities of the sample (Figure 11C and D) and silica spheres of patterned nanocomposite prior to wet etching (Figure 11E) are evident. RIE can also be used to pattern polymerized nanocomposite films. Due to isotropic etching of the RIE process, slanted surfaces of ordered spheres with well-defined angles are formed (Figure 11F). These angled sidewalls can be used as reflective mirrors to couple light out of the planar devices for potential optical and optoelectronic on-chip integration.[74]

Conclusions

We have demonstrated the formation of high-quality, large-area, 3D ordered nanocomposites, colloidal crystals, and macroporous polymers with controllable thickness by a simple and fast spin-coating process. Sample as large as four-inch diameter can be routinely created within minutes, and the crystalline qualities are not compromised by the fast fabrication process. The on-wafer planar configuration, highly uniform thickness and compatibility with contemporary microfabrication of this technique may make the eventual mass production of low-cost practical devices, ranging from photonic crystals to high-density optical recording materials to bio-separation membranes, possible. Besides important technological applications, our process opens a new route to the fundamental study of shear-induced crystallization.

Supporting Information Available: A video clip showing the colloidal crystallization process by spin-coating. This material is available free of charge via the Internet at http://pubs.acs.org.

(71) Jethmalani, J. M.; Ford, W. T.; Beaucage, G. *Langmuir* **1997**, *13*, 3338–3344.
(72) Yethiraj, A.; van Blaaderen, A. *Nature* **2003**, *421*, 513–517.
(73) Busch, K.; John, S. *Phys. Rev. E* **1998**, *58*, 3896–3908.
(74) Gan, J. H.; Wu, L. H.; Luan, H. F.; Bihari, B.; Chen, R. T. *IEEE Photonic Technol. Lett.* **1999**, *11*, 1452–1454.

JA0470923